Hindawi Publishing Corporation
Journal of Nanomaterials
Volume 2012, Article ID 890701, 11 pages
doi:10.1155/2012/890701

Research Article

On the Origin of Light Emission in Silicon Rich Oxide Obtained by Low-Pressure Chemical Vapor Deposition

M. Aceves-Mijares,[1] A. A. González-Fernández,[2] R. López-Estopier,[3] A. Luna-López,[4] D. Berman-Mendoza,[5] A. Morales,[6] C. Falcony,[7] C. Domínguez,[2] and R. Murphy-Arteaga[1]

[1] *Department of Electronics, INAOE, 72840 Puebla, Mexico*
[2] *Department of Micro and Nanosystems, IMB-CNM (CSIC), 08193 Barcelona, Spain*
[3] *Department of Applied Physics and Electromagnetism, University of Valencia, 46100 Burjassot, Spain*
[4] *Research Center for Semiconductor Devices, Autonomous University of Puebla, 72570 Puebla, Mexico*
[5] *Departamento de Investigación en Física, Universidad de Sonora, 83000 Hermosillo, SON, Mexico*
[6] *Centro de Investigación en Materiales Avanzados S.C., Unidad Monterrey-PIIT, 66600 Apodaca, NL, Mexico*
[7] *Department of Physics, CINVESTAV-IPN, 07360 Mexico City, DF, Mexico*

Correspondence should be addressed to M. Aceves-Mijares, maceves@inaoep.mx

Received 19 January 2012; Revised 29 March 2012; Accepted 13 April 2012

Academic Editor: Jai Singh

Silicon Rich Oxide (SRO) has been considered as a material to overcome the drawbacks of silicon to achieve optical functions. Various techniques can be used to produce it, including Low-Pressure Chemical Vapor Deposition (LPCVD). In this paper, a brief description of the studies carried out and discussions of the results obtained on electro-, cathode-, and photoluminescence properties of SRO prepared by LPCVD and annealed at 1,100°C are presented. The experimental results lead us to accept that SRO emission properties are due to oxidation state nanoagglomerates rather than to nanocrystals. The emission mechanism is similar to Donor-Acceptor decay in semiconductors, and a wide emission spectrum, from 450 to 850 nm, has been observed. The results show that emission is a function of both silicon excess in the film and excitation energy. As a result different color emissions can be obtained by selecting the suitable excitation energy.

1. Introduction

Silicon Rich Oxide (SRO) is a multiphase material composed of elemental Si, SiO_2, and SiO_x, with x between 0 and 2. DiMaria and coworkers distinguished between low and high density of elemental silicon (or silicon excess); films with low silicon excess were named "off stoichiometric oxide" [1]. Also, they did not find nanocrystals (nCs) in SRO annealed at 1,000°C with a 5-6 % silicon excess.

SRO can be obtained in different ways. However, (chemical vapor deposition) CVD and Si implantation into silicon oxide are the most common techniques. (Low-Pressure CVD) LPCVD is a simple method that easily allows varying the silicon excess [2]. In this technique, the flux ratio of reactive gases, Ro, is used to determine the silicon excess. Silane (SiH_4) and nitrous oxide (N_2O) are commonly used:

$$\mathrm{Ro} = \frac{N_2O}{SiH_4}. \quad (1)$$

It is known that Ro = 3 produces an excess of silicon of 17%, and Ro > 100 is used to obtain stoichiometric silicon dioxide [2]. In the case of SRO fabricated by silicon implantation, silicon excess is related to the implantation dose.

SRO has been a matter of intense research due to its optical properties. SRO is totally compatible with MOS technology, and it has thus been used to overcome the limitations of silicon as an indirect material. DiMaria et al. observed emission of light by SRO for the first time [1], and researchers have been finding practical applications

for its properties ever since. Nevertheless, the number of applications is still reduced since the emission mechanisms are not completely understood. Nowadays, however, most of the authors accept that quantum effects in nanocrystals, and defects in the SiO_x matrix, are responsible for the emission of light [3].

Silicon nanocrystals have been commonly observed in high silicon excess SRO, higher than 10%. However, in LPCVD SRO, the highest light emission has been observed in films with silicon excess in the order of 5%, in which nanocrystals have not been observed [1, 4, 5]. Therefore, in low silicon excess the emission characteristics can be related to silicon, or silicon oxidation states, specifically to amorphous nanoagglomerates (Si nanopoints). Therefore, for low silicon excess SRO the dominant mechanism is not quantum confinement.

In this paper a review of our work on the different structural characteristics of SRO obtained by LPCVD is presented. Next, using experimental results of photo-, cathode-, and electroluminescence, a discussion of SRO emission mechanisms is presented. Finally, Donor-Acceptor decay is proposed to explain the emission mechanisms of the three excitation methods.

2. Experimental

All samples were obtained by LPCVD; the ratios Ro of reactive gases were 10, 20, and 30 (SRO10, SRO20, and SRO30), corresponding to approximately 12, 7, and 5% of silicon excess, respectively. A hot wall chamber was used, and the temperature was approximately 700°C. After deposition, the samples were annealed at 1,100°C in nitrogen gas for 180 minutes; however some samples underwent shorter annealing times; for these cases the annealing time will be indicated. In the following sections, references to our previous work are cited, and we suggest to the interested reader to refer to them to obtain more general details on experimental settings.

3. Results and Discussion

3.1. Silicon Excess. SRO silicon excess was measured by (X-Ray Photoelectron Spectroscopy) XPS and (Rutherford Backscattering Spectroscopy) RBS. Both techniques are used to determine the elemental composition of films. For more details on the characterization techniques, you can see, for example, [6]. With the RBS technique, Si can normally be detected up to 0.001%, whereas with XPS only to 0.1%. XPS can also be used to determine the Si oxidation states. Table 1 shows the compositional results of the SRO10, SRO20, and SRO30 samples (SRO with Ro = 10, 20, and 30, resp.). Note that only two samples were measured by RBS.

The microstructure of SRO films was studied analyzing the Si2p spectra, according to the Random Bonding Model [7]. The Si2p XPS peaks were decomposed considering the five possible oxidation states for silicon: Si, Si_2O, SiO, Si_2O_3, and SiO_2. Each oxidation state was fitted using Gaussian distributions, and the energy positions of the different peaks were centered with those previously reported in the literature at ~99.8, 100.5, 101.5, 102.5 and 103.5 eV [8, 9]. The full widths at half maximum (FWHM) were allowed to vary within a small range [10, 11]. The relative concentration of each oxidation state was determined and is presented in Table 2 [12, 13].

Dong et al. [2], using electron microprobe analysis, determined the silicon excess in as-deposited atmospheric pressure CVD SRO films. The reactant gases were SiH_4 and N_2O, the same ones used in this study. For Ro ratios varying between 3 and 100, they found a silicon variation between 45 and 33%, respectively, which is 12 to 0 at.% Si excess. Based on the Dong results, it is accepted [4] that for APCVD and LPCVD (atmospheric and low pressure CVD, resp.) SRO films with Ro = 10, 20, and 30 correspond to silicon excesses of approximately 12, 7, and 5%.

The silicon excess results shown in Table 1 agree with those obtained by Dong. Hence, for the SRO films obtained by LPCVD with N_2O and SiH_4 as reactant gases, silicon excesses can be taken as 12, 7, and 5 at.% for Ro = 10, 20, and 30, respectively. Additionally, comparable optical and morphological properties were observed for SRO with silicon excess in a specific range. So, a high silicon excess range can be defined for Ro < 10, or silicon excess higher than 10 %. The medium silicon excess range is defined for Ro between 15 and 35, or silicon excess between 9 and 3 at.%. Finally, the low silicon excess range, for Ro > 40, or silicon excess between 2 and stoichiometric oxide, is defined. Then, the high range of silicon excess is distinguished by SRO films that show a high density of large nanocrystals, high electronic current and low light emission. On the other hand, the medium silicon excess range has a very low density, or none, of small nanocrystals and intense light emission. At the other extreme, low silicon excess SRO behaves as a stoichiometric oxide.

3.2. Nanocrystal Structure

3.2.1. X-ray Diffraction. (XRD) is mainly used to determine the crystal structure of solids, powders, and colloidal solutions. In our studies, XRD was used to determine if nanocrystals were embedded in the different SRO layers. Figure 1 shows the X-ray diffraction peaks for SRO films with different silicon excesses. For a high silicon excess, 12%, the nanocrystalline evidence is clear, whereas for a silicon excess of about 7% small peaks are still observed. However, for a silicon excess less than 6%, no crystalline evidence was observed [14].

In [15], an XRD study of films with medium to high silicon excesses obtained by (Plasma Enhanced CVD) PECVD and annealed at high temperature showed that as silicon increases, silicon nanocrystal density and size increase. However, for the smaller percentage of silicon in the film higher temperatures and longer times are needed to detect silicon crystals. This agrees well with our XRD observations, as shown in Figure 1. For SRO10, high Si excess range, the (220), and specially (111) crystalline orientations are clearly observed. As the silicon excess is reduced from SRO10 to

Table 1: Compositional results of SRO annealed at 1,100°C (TT) and as-deposited.

Ro	TT 1100°C	XPS Si excess at.%	XPS $x = O/Si$	RBS Si excess at.%	RBS $x = O/Si$	AFM Roughness (nm)
30	No	4.54	1.61	5	1.605	8
30	Yes	4.21	1.63	NA	NA	5
20	No	5.38	1.54	7	1.475	10
20	Yes	5.09	1.54	NA	NA	6
10	No	13.50	1.09	NA	NA	17
10	Yes	14.50	1.01	NA	NA	24

Table 2: Concentration of oxidation states for the SRO samples according to the random bonding model.

Oxidation state	Ro = 30	$R = 20$	$R = 10$
SiO_2%	47.35	42.89	45.86
Si_2O_3%	23.04	29.39	19.42
SiO %	19.57	18.23	13.02
Si_2O %	7.94	6.65	10.53
Elemental Si %	2.10	2.84	11.18

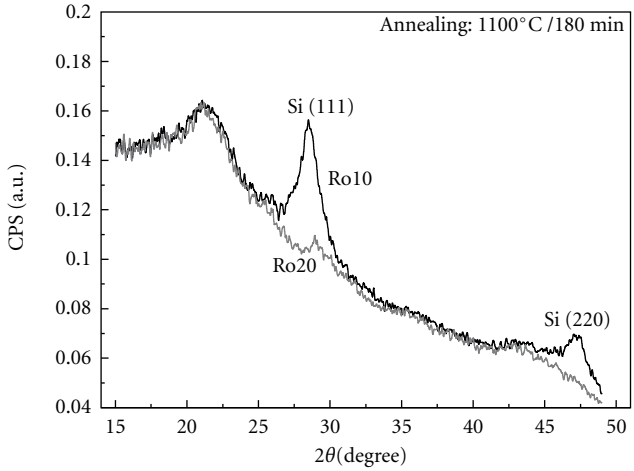

Figure 1: XRD results for SRO film with different silicon excesses; high silicon excess, 12%, clearly shows a crystalline phase. As the silicon excess is reduced, nano-crystal density is reduced until it disappears.

SRO20, the SiO_2 phase does not change, and the Si crystalline phase is scarcely observed. As the Si is further reduced, no evidence of any crystalline structure was detected.

3.2.2. Transmission Electron Microscopy. (TEM) observations were also performed for SRO with Ro = 10, 20, and 30, and the images were used to corroborate the presence of nanocrystals in the SRO films. At relatively low amplification, the absorption of electrons in the material is enough to produce an image. However, at higher magnifications, phase contrast is required for (high resolution TEM) HRTEM, and small non-crystalline particles are not easily observed [16].

Figure 2 shows a TEM image and a diffraction pattern of an SRO film with a silicon excess of 12%; silicon nanocrystals are clearly observed [17, 18]. The nanocrystal sizes are between 2 and 10 nm, the average size is around 5 nm, and their density is around $1.0 \times 10^{12}\,\text{cm}^{-2}$. However, for low silicon excesses, less than 6%, no nanocrystals were observed using high-resolution TEM. Nevertheless, using EFTEM, silicon agglomerates were observed for a 7% silicon excess, whereas for a 5% silicon excess not even these agglomerates were observed even though a silicon excess was corroborated by XPS.

Iacona et al. [19] have also done EFTEM studies on high silicon excess SRO obtained by PECVD. Their results show that after annealing a phase separation is observed, and crystals develop from amorphous homogeneous SiO_x. Similar to our results for the high Si excess films, large nanocrystals are observed after thermal annealing; in the upper limit of the medium excess range some small nanocrystal are still observed, but as the silicon excess is reduced it is not possible to detect nanocrystals at all [18].

3.2.3. Atomic Force Microscopy. (AFM) surface images of SRO films were obtained for all the samples studied; the typical roughness is shown in Table 1. Figures 3 and 4 show the AFM images and height profiles of SRO10 and SRO30. They look granular, and the grain size increases as the Ro is reduced, which indicates that the roughness should be proportional to the presence of silicon nanocrystals, as demonstrated by XRD and TEM. The roughness increases for the high Si excess films after annealing. For low silicon excesses, however, the roughness is reduced after thermal annealing [13]. This is an indication that after annealing, nanocrystals grow in high silicon excesses, while in the medium excess range formation of Si–O compounds takes place.

3.3. Molecular Analysis

3.3.1. Fourier Transform Infrared Spectroscopy. (FTIR) gives information of the molecular absorption; therefore it allows the study of the fundamental vibrations and associated rotational-vibrational structure. SRO films show characteristic infrared absorption peaks associated with the Si–O–Si bonds in SiO_2 [12, 20, 21]. The FTIR absorbance spectra of SRO samples are pictured in Figure 5 and were identified as (1) Si–O rocking at ~450 cm^{-1}, (2) Si–O bending at

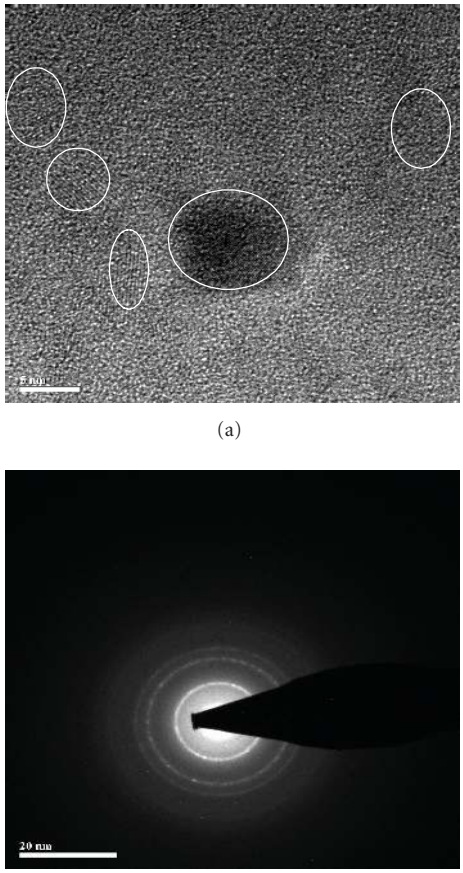

(a)

(b)

Figure 2: TEM images (a) and diffraction pattern (b) of a selected area of the annealed SRO film with a 12% silicon excess. Silicon nanocrystals are clearly observed.

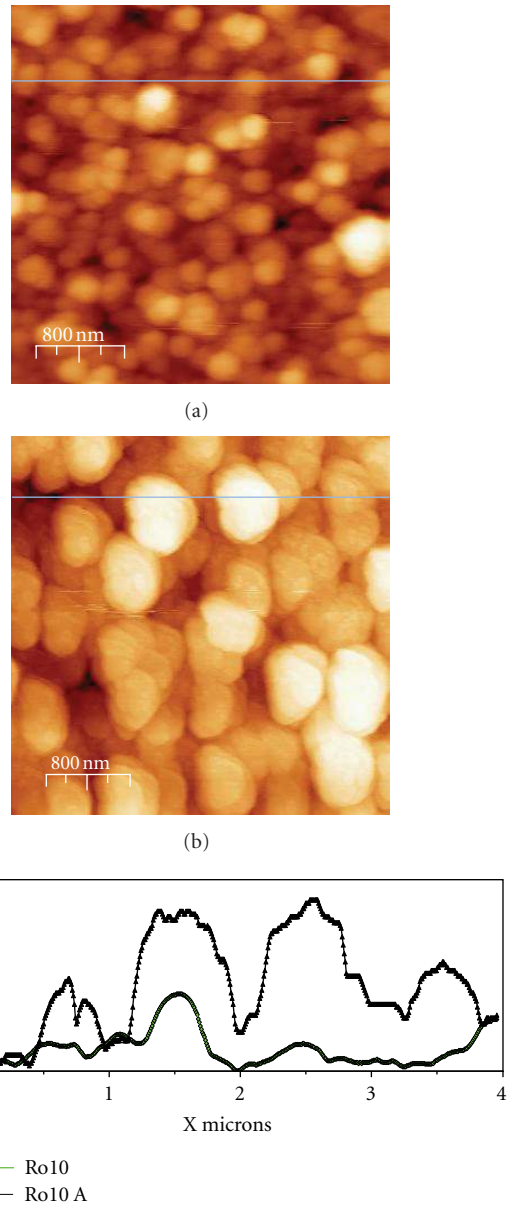

(a)

(b)

(c)

Figure 3: AFM images of SRO10 (a) as-deposited and (b) after annealing at 1,100°C for 180 minutes (Ro10 A), and (c) comparison of profiles along the lines in the images.

~808 cm^{-1}, (5) Si–O symmetric stretching vibration from 1055 to 1082 cm^{-1} and (7) Si–O asymmetric stretching at ~1170 cm^{-1}. In addition, (3) Si–H bending at ~883 cm^{-1}, (4) Si–N stretching at ~984 cm^{-1}, and (7) Si–H stretching at ~2258 cm^{-1} bonds were also found in SRO samples [22, 23]. The inset in Figure 5 shows Si–N and Si–H bonding before and after annealing.

The as-deposited samples exhibit a characteristic IR absorption due to the stretching vibration of the Si–O–Si bonds around 1060–1055 cm^{-1}; the absorbance and frequency of stretching vibration peaks decrease as Ro decreases. Figure 6 shows the behavior of the Si–O stretching peak frequency for samples with different silicon excesses. The frequency is lower than that for an SiO_2 film (1080 cm^{-1}) and that of an amorphous a-SiO_2 film (1074 cm^{-1}) because Si atoms replace O atoms [21]. This result is related to the off-stoichiometry of SRO, which causes a decrease in the stretching frequency of Si–O as the x in SiO_x decreases (silicon excess increases). For all samples, the stretching frequency increases after annealing for all silicon excesses, as also shown in Figure 6. This result suggests a phase separation during the thermal annealing and an increase of oxidized compounds from the oxide phase.

It has been reported that SRO films deposited with a mixture of N_2O and SiH_4 display absorption bands associated with Si–H (660, 880, and 2250 cm^{-1}), Si–N (870–1030 cm^{-1}), Si–OH (940, 3660 cm^{-1}), and N–H (1150, 1180, and 3380 cm^{-1}) in addition to the three characteristic bands related to the Si–O–Si bonding arrangement [21, 24]. The presence of some nitrogen and hydrogen characteristic peaks has been also observed in the IR spectra of our films. Si–H bending and stretching were observed only in as-deposited samples; these peaks disappear after annealing due to the high-temperature treatment. Si–N stretching was also found in both as-deposited and annealed samples.

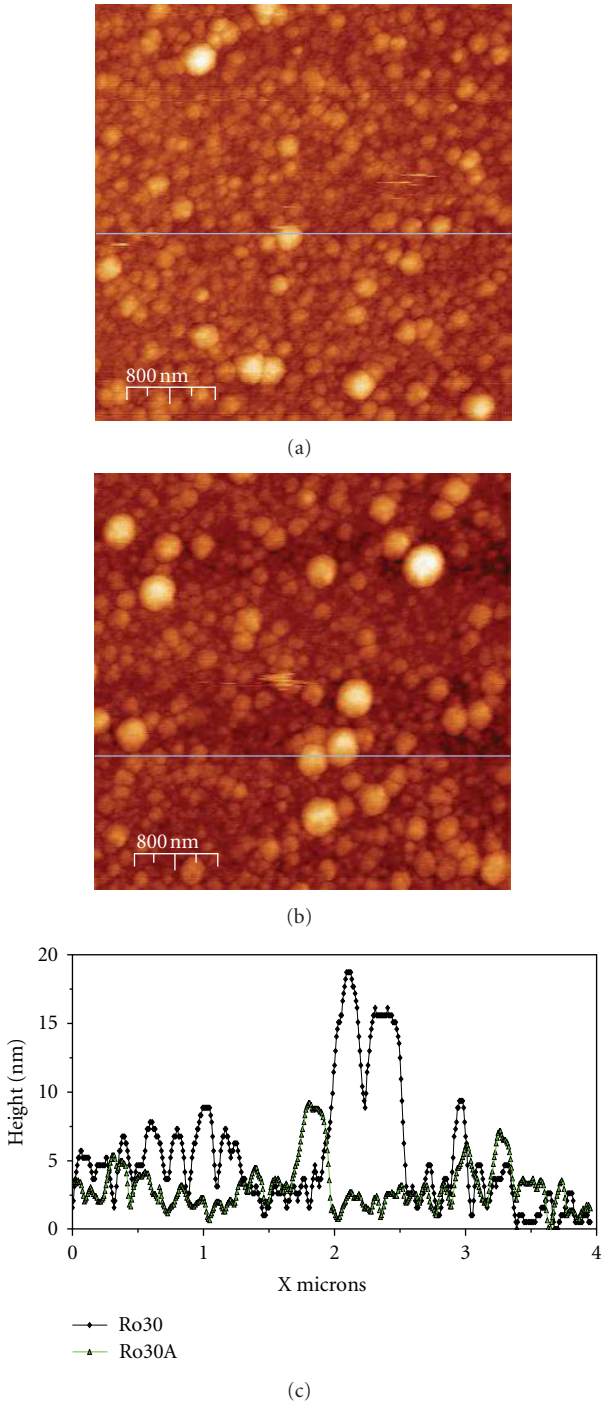

Figure 4: AFM images of SRO30 (a) as-deposited and (b) after annealing (Ro30 A) at 1,100°C for 180 minutes, and (c) comparison of profiles along the lines in the images.

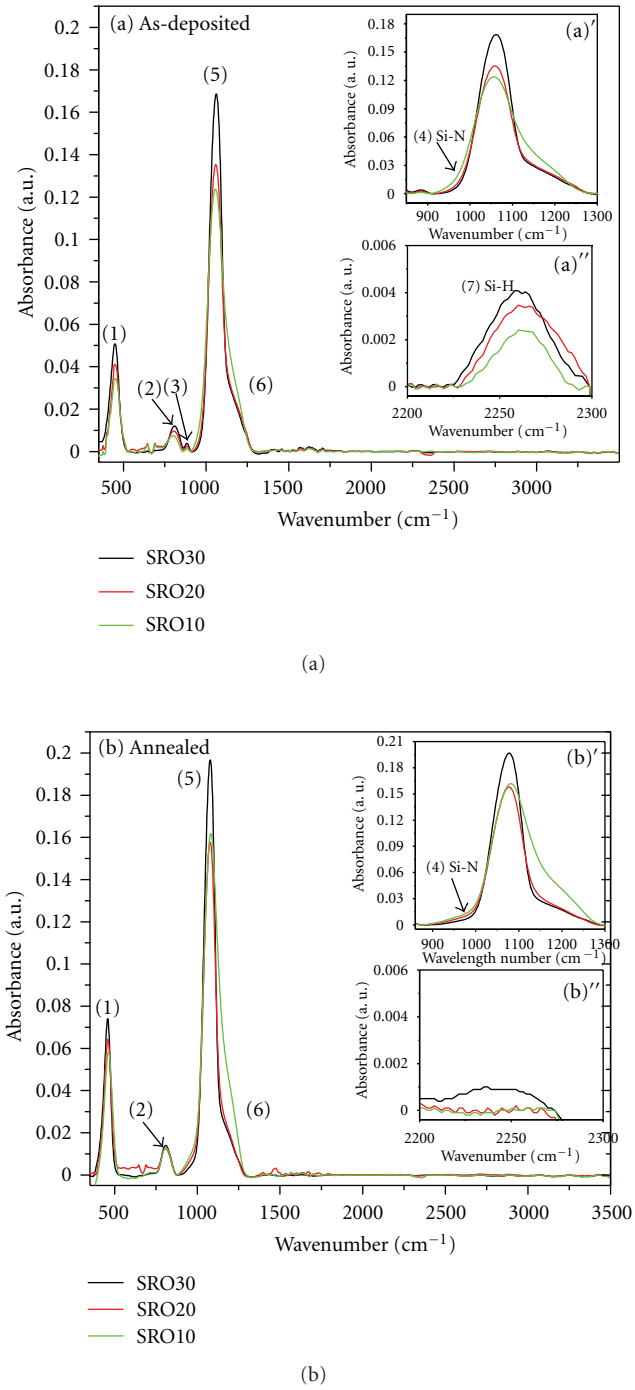

Figure 5: FTIR absorption spectra of SRO films (a) before and (b) after thermal annealing. The inset shows Si–N and Si–H bonding in the 850–1300 cm^{-1} and 2200–2300 cm^{-1} ranges, respectively.

Having analyzed the LPCVD-SRO in the three ranges of silicon excess, there is enough evidence to suppose that annealing at 1,100°C produces a phase separation of elemental silicon, SiO_x, and SiO_2. Depending on the silicon excess, the amount of each phase increases notoriously, as can be seen in Table 2. It is clear that in the high range the quantity of elemental silicon is the highest, 11% for SRO10 and only 2% for SRO30. However, SiO_x is as high as 54% for medium silicon excesses and only 40% for SRO10. The percentage of SiO_2 is similar for the high and medium ranges.

It is clear then that two competitive morphological mechanisms take place during annealing; one is the formation of silicon agglomerates, and the other is the formation of silicon and oxygen compounds. If silicon excess is high enough, the

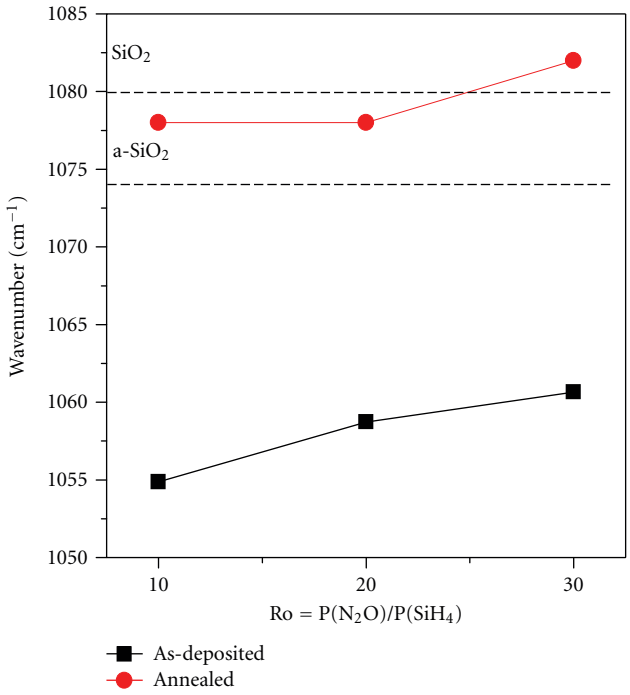

Figure 6: Si–O stretching frequency positions for different Ro, for SRO films before and after annealing at 1,100°C for 180 minutes.

silicon agglomerates will morph into nanocrystals. As Si is decreased, however, silicon oxidation states will dominate due to the larger separation between elemental silicon. As silicon excess increases, the SRO will tend towards a polysilicon layer; conversely, as silicon is reduced, the SRO film will move towards a stoichiometric SiO_2. In between these extremes, agglomeration of silicon shifts towards the agglomeration of Si-oxygen compounds as the silicon excess moves from high to low silicon excesses.

3.4. Luminescence. The low-temperature emission of light from electronically or vibrational excited species is known as luminescence [25]. Depending on the excitation, it receives different names; for instance, when the excitation energy is due to photons, the emission mechanism is called photoluminescence. When emission is produced by an electric current passing through the sample, Electroluminescence, EL, is obtained. Cathode-luminescence, CL, is produced when an electron beam is accelerated and implanted into the sample. Thermoluminescence, TL, arises when electrons trapped in a sample are released by heat and then recombine emitting light [26]. SRO obtained by LPCVD and annealed at 1,100°C has shown PL, CL, EL, and TL [27].

Luminescence from samples can deliver significant information regarding the structure of a material; in the case of SRO, luminescence studies are particularly important, given the fact that these films are specifically seen as a light-emitting material. As mentioned previously, the first ones to observe luminescence in LPCVD SRO were DiMaria et al., but since then, Canham observed PL from porous silicon in 1990. The photoemissive properties of this material, along with those of others based in nanostructurated Si such as SRO, have been extensively studied since. Despite these efforts, no clear consensus has been reached regarding the origin of luminescence, but recently, it has been generally accepted that it is due to a combination of quantum phenomena and defect-related emission [1, 28–30]. Electro- and cathode-luminescence studies are more complex than PL, because carriers are injected to the material; therefore luminescence can be either due to relaxation of higher-energy carriers through radiative centers or due to the recombination of excitons formed by impact ionization by the injected carriers [31, 32].

3.4.1. Photoluminescence (PL). spectra are obtained stimulating the samples with light in order to transfer energy to carriers that will later relax and radiatively recombine. The simple model proposes that recombination centers are distributed in the photoluminescent material, and these centers increase the probability of radiative recombination. The energetic distribution of such centers can be extracted when analyzing the emission spectra. The stimulation energy can also be varied in order to identify the absorption centers.

In this report, photoluminescence (PL) emission spectra were obtained pumping the samples with UV radiation with a wavelength of between 250 and 360 nanometers, measured between 400 and 900 nm. Absorption (or excitation) spectra were also obtained, stimulating the samples with light ranging from 200 to 400 nm and detecting the emission at a given wavelength. Figure 7 shows the emission spectra and Figure 8 shows the absorption spectra with the detector at 750 nm for SRO10, 20, and 30. Neither aged samples nor samples deposited at different times produce significant emission variations. In the as-deposited samples, there is practically no emission; only the SRO30 samples indicate a small emission in the range of 450 nm. Therefore, the discussion will be centered on the samples annealed at 1,100°C for 180 minutes, and the small peak at 450 nm will be discussed later.

The highest emission is obtained from SRO30 samples; as demonstrated in the morphological details, these samples do not show evidence of nanocrystals, and rather they contain Si–O compounds. Hence, the emission can be attributed to the oxidation states or defects. It is possible that during annealing, the defects agglomerate forming emission centers; for example, emissions at 460 nm, 520 nm, and 650 nm have been related to oxygen deficiency-related centers (ODCs) or oxygen vacancies [12, 33]. Besides, it has also been demonstrated that the electronic characteristics in SRO are due to traps [34, 35]. Then, in the medium range of silicon excess, the photoexcited electrons will jump to the traps leaving a positive mirror charge behind, and the Coulombic attraction promotes the decay of electrons producing emission. Naturally, there should be an optimum silicon excess density that produces the maximum emission, and according to our studies, this is around 5% silicon atomic excess. On the other hand, as the silicon excess increases, more nanocrystals grow, and less traps are obtained. As a result, the emission is reduced and the conductivity increases. In the high excess Si range the conduction is by tunneling through nanocrystals

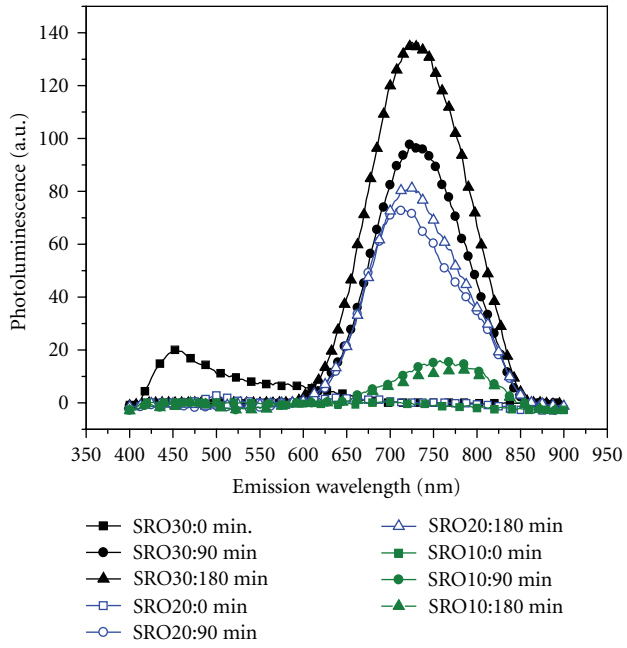

Figure 7: Photoluminescence for SRO10, 20, and 30 before and after annealing at 1,100°C for the time shown in the legend, for an excitation wavelength of 270 nm. No significant peak shifts are observed with time or with silicon excess.

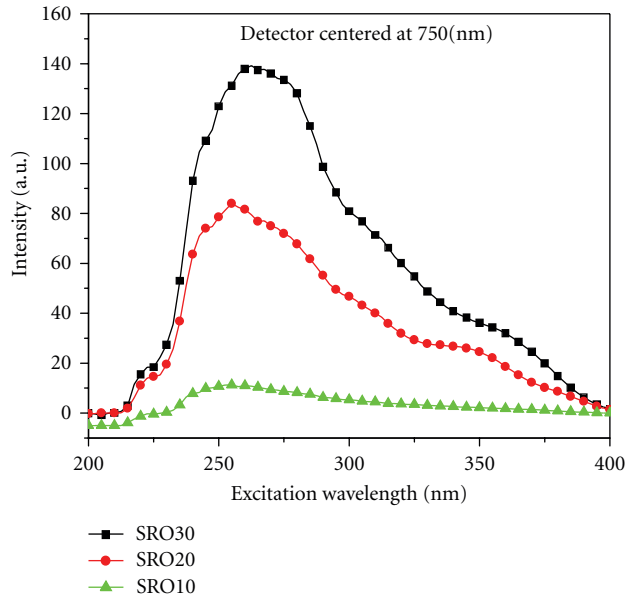

Figure 8: Excitation wavelength with the detector centered at 750 nm for SRO10, 20, and 30 annealed at 1,100°C for 180 minutes.

[36]. In the nanocrystals the electrons will move in the conduction band, or they will nonradiatively recombine. Consequently, in the high range of silicon excess, most of the excited electrons will move, or decay without radiating, through the abundant nanocrystals, and only a few of them will find the rather scarce traps. Consequently, low emission is expected. In [37] the authors also propose that even for very small Si crystallites the bandgap remains indirect.

Figure 8 displays the wide excitation spectra for SRO10, 20, and 30. It does not exhibit the expected absorption peaks and the blue shift of an excitonic absorption. The observation of nonexcitonic absorption spectra for Si nanocrystals has been also reported by other authors [38].

Furthermore, from Figure 7 it is clear that as the Ro varies from 10 to 30, the SRO emission bands do not shift significantly to higher energies, as the size of the nanocrystals is reduced, notwithstanding the considerable size variation of the Si nanoagglomerates, crystalline, or not. However, in reports where emission is attributed to Si nanocrystals, wavelength shifts of hundreds of nanometers for smaller differences in the nanocrystal size have been experimentally corroborated [37, 39]. Additionally, a shift toward the blue side of the spectrum caused by different excitation energies has been reported. For example, in the study of nanocrystal PL emission in colloidal suspensions, green emission that shifts toward higher energies was observed when the incident photon energy was increased [40], but the authors mention that the Wolking model cannot be used to explain their results [41]. Wolking proposes that, in the emission of porous silicon, carriers are trapped in silicon oxide bonds, which explains the 2.1 eV limit energy in nanocrystals smaller than 3 nm.

3.4.2. Electroluminescence (EL). increases the energy of emission since electrons are injected into the conduction band and holes into the valence band, allowing band edge emissions. Therefore, electro-luminescence can be due to relaxation of higher-energy carriers through radiative centers [42].

Electro-luminescence was tested in devices having a MOS-like structure, using polysilicon as the gate electrode (Light-Emitting Capacitor, LEC). Polysilicon is transparent enough in the emission range of SRO [43]. EL in SRO obtained by LPCVD and annealed at 1,100°C requires a high applied electric field and high currents, and thus these devices work close to the electrical damage point. Only devices that show high photoemission show electroemission; therefore, only devices with a medium silicon excess are suitable for EL. Figure 9 shows the EL emission spectrum of a capacitor with SRO30 as a function of applied voltage. Two peaks are very well defined; one centered at around 450 nm (blue emission), and the other around 700 nm (red emission). The peak intensity varies with the applied voltage; one shows a higher increment than the other, and a slight shift toward higher energies is observed. The spectrum of the one around 700 nm is similar to the one obtained with PL.

Figure 10 shows the percentage of intensity of each peak to the total emission. Total emission was obtained simply by adding the peak intensity of the red and blue peaks in arbitrary units. From the figure it is clear that the percentage of red emission is reduced as the electric field increases, and the percentage of blue emission increases with voltage. That is, as the applied energy increases, the part of the emission corresponding to the blue range is practically the

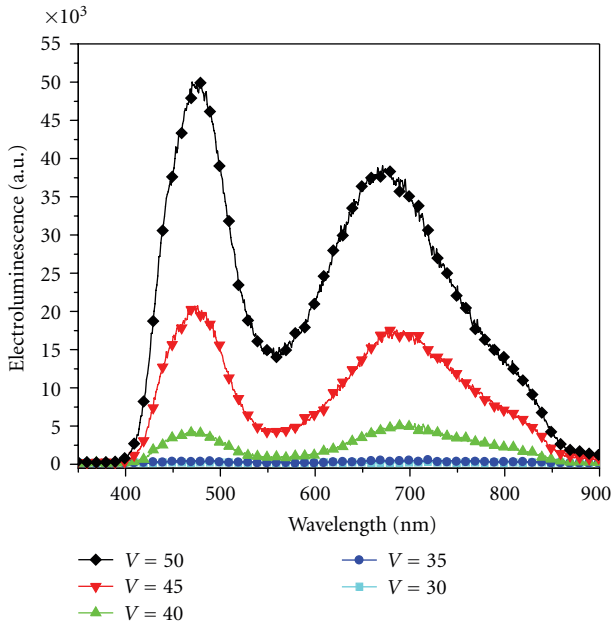

Figure 9: Electroluminescence versus wavelength as a function of applied voltage of a MOS-like structure with SRO30 and polysilicon as the gate electrode. As can be seen, two emission ranges are well defined. The intensity peaks vary with the applied voltage (V).

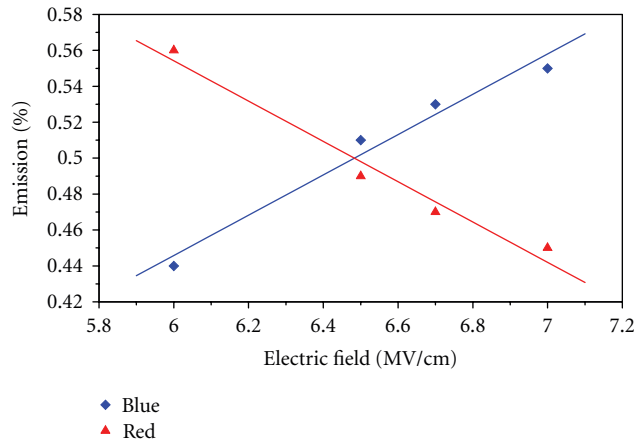

Figure 10: Percent of the total intensity emission of the blue and red peaks of Figure 9; the red emission tends towards 0 as the electric field increases and the blue emission tends to be the only one at high electric fields. The total emission was obtained adding the two peak intensities in Figure 9.

total emission (100%), and the red part is reduced towards 0%. This is corroborated when a very high energy is used, for example, in cathode-luminescence. The systematic variation of the spectra with energy indicates that the double emission is not due to the presence of singlets and triplets.

When electrons are injected into the SRO in the LEC, the charge is distributed among the cluster of defects, or Si–O compounds, which act as shallow and deep traps that behave as emission centers of low and high energy (red and blue), respectively. As it is known, the mobility of electrons in the SRO is very high compared with that of holes; it is then likely that the emission is due to electrons decaying into positive traps. The emission mechanism of an LEC is quite similar to that observed in organic light emitting diodes which also have a high distribution of traps [44].

In the medium silicon excess range especially, when electrons are injected from one electrode into the SRO by an electrical potential difference, they move through the film to the other electrode, and, as known [35], a fraction of them will be trapped. As the current increases, trapped electrons will block the conduction paths. Trapped electrons accumulate and consequently decay towards empty positive traps, in a similar fashion as the donor-acceptor pair decays in semiconductors [45]. The higher the applied voltage, the higher the energy driving the electrons is, and then the deep traps are reached, and more energetic photons are emitted.

From the morphological point of view in the medium Si excess films, the agglomerates of defects are constituted by compounds, which require different, higher or lower, energy to be excited. Then, at low electric fields, or using UV radiation, most of electrons will be trapped at lower energies, producing emission mainly in the red side of the spectrum, as shown in Figure 9. As the applied energy is increased, more energetic compounds will be excited, or electrons are trapped in more energetic states, and when they relax, the blue emission becomes dominant.

Clearly, to obtain electroluminescence in LECs made of SRO obtained by LPCVD and annealed at 1,100°C three conditions have to be met: the density of Si–O compounds has to be high, the energy applied to the LEC has to be high enough to reach the different energetic states, and there must be a high injection of carriers from one electrode to produce agglomeration of electrons in the conduction trajectories in the film.

Cathode-Luminescence. (CL) is obtained when light is produced using a beam of high-energy electrons. CL is a technique that normally leads to emission by all of the mechanisms present in the material, and then CL, PL, and EL can be compared to complement the information in order to have more details of the emission properties of luminescent materials [46].

Cathode-luminescence spectra were obtained under different bombardment conditions. Figures 11 and 12 show the cathode-luminescence spectra of SRO10, 20, and 30 before and after annealing at 1,100°C for 180 minutes. As can be observed, the CL spectra of the as-deposited samples are similar to those of PL, and only emission at around 450 nm is observed for SRO30 films. From CL and PL results it can be inferred that no other but blue emission centers are present in the as-deposited samples. Because there are not any more centers, no competition takes place, and even when UV radiation impinges on the samples, blue emission is obtained. When the silicon excess shifts towards higher-density ranges, the amount of blue centers is reduced and emission is quenched.

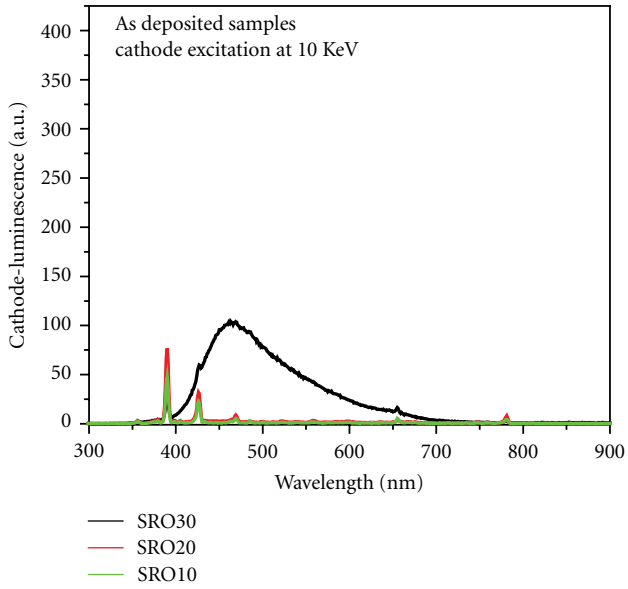

Figure 11: Cathode-luminescence spectrum for SRO10, 20, and 30 as-deposited films.

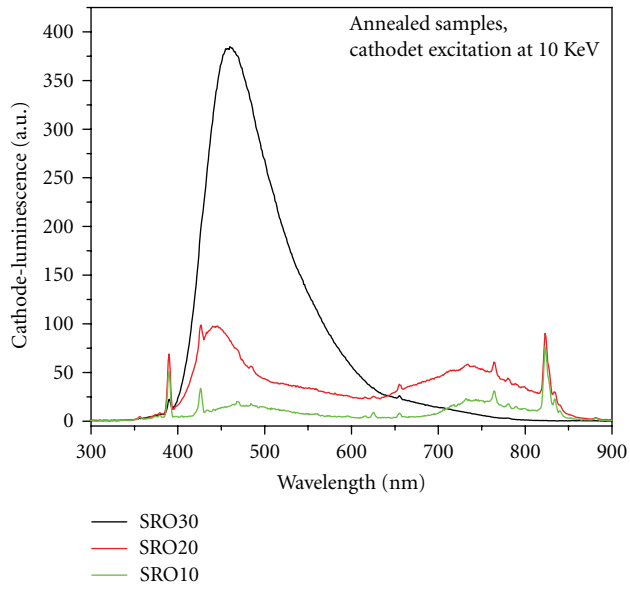

Figure 12: Cathode-luminescence for SRO10, 20, and 30 after annealing at 1,100°C for 180 minutes.

On the other hand, after annealing, more blue and red centers are produced, and emission in the red side increases. For PL of SRO30 and 20 the photoelectrons will only reach red centers, and red emission becomes dominant. However, more energetic cathode-electrons will reach both blue and red centers, causing emission of both colors, with blue dominating.

As already mentioned, the annealing produces a phase separation that agglomerates Si–O compounds and its density increases until an optimum is reached, corresponding to the medium density silicon excess films. This is particularly clear in Figure 12; in SRO10 low CL emission in red and blue is obtained, showing a slightly higher peak in the red side than in the blue, which means that red and blue density centers are comparable. As Ro increases towards SRO20, the emission in the blue side clearly shows a higher increase than red emission, indicating that the quantity of blue centers was increased at a higher rate than the red centers. Since the density of blue centers is not very high, the cathode electrons are shared between both the blue and red centers, producing both emissions. When SRO30 was excited with high-energy electrons, the blue emission became completely dominant. As a consequence of the higher density of blue centers that appears after annealing, the blue centers collect more of the high-energy electrons and only a few reach to the red centers.

Since different equipment and arbitrary units are used, it is not possible to compare the CL and PL emissions directly, but this could be a method to determine the density of emission centers. On the other hand, due to the fact that no UV emission was observed in CL, in spite of the very high energy used, it is evident that no UV centers are produced in the SRO films.

Figure 13 compares the most representative PL, CL, and EL normalized spectra. A blue shift clearly occurs as the excitation energy increases, and emission centers of a wide color spectra (from 450 to 850 nm) are observed in the SRO films obtained by LPCVD and annealed at 1,100°C. Therefore, 450 to 850 nm emission centers evolve with the annealing. As implied in Figure 12, for SRO30, the density of blue centers is the highest. Then, as can be observed from CL, PL, and EL, the as-deposited SRO30 film already presents blue emission centers, and after annealing many other centers evolve specially in the medium Si excess range; that is, the density of blue centers increases, followed by the density of red centers. However, the density of green centers of around 550 nm is the smallest one.

From Figure 13, it is also clear that when the energy increases, high-energy emission centers are reached; however the density of such centers limits the emission. Then, CL for SRO30 emits basically in the blue region because the blue center density is the highest. As the silicon excess increases, the density of blue centers is reduced and blue and red emissions compete, as in the case of CL in SRO20. Correspondingly for EL, red and blue emissions compete as a function of applied energy. At low voltages, low peaks of similar intensity of both colors are observed; however when the voltage is increased, a clear blue shift is observed and the blue emission increases more than the red one. PL, on the other hand, is pumped with relatively low-energy photons, producing low-energy photoelectrons that cannot reach the high-energy blue centers, and emitting only in the red part of the spectrum. Then, blue-to-red emission of different intensities can be observed for the medium silicon excess range.

In the high-density range, as for the SRO10 films, the emission centers barely develop. Consequently, for this range almost no emission is observed. Therefore, the light emission in SRO annealed at 1,100°C will be a function of the excitation energy and silicon excess. Therefore, a specific color emission can be selected as a function of the applied voltage exploiting EL.

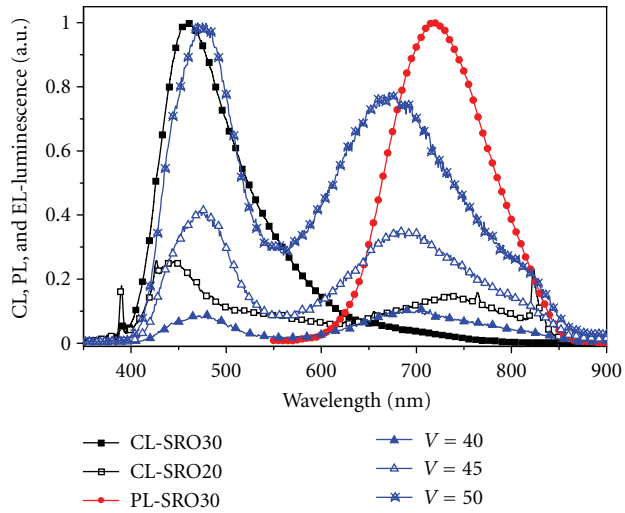

Figure 13: Normalized electro-, cathode- and photoluminescence of SRO with more representative silicon excesses. CL is shown for SRO20 and 30, PL and EL is shown for SRO30, and EL is shown for three different voltages.

4. Conclusions

Structural and emission properties of SRO films, of high and medium silicon excess density, obtained by LPCVD and annealed at 1,100°C were studied. Three ranges of silicon excess were defined, in which the SRO shows similar characteristics. After annealing, the high-density range is characterized by the agglomeration and crystallization of elemental silicon, so its characteristics are dominated by nanocrystals, with more conductive paths and lower light emission. Medium Si density is characterized by a high number of Si–O compounds that act as emission centers, and then light emission is easily stimulated. Additionally, the SRO emission spectrum is wide, in the range from 450 to 850 nm. The emission depends on excitation energy and on the density of Si compounds (or silicon excess). The highest emission was obtained for SRO with a silicon excess around 5 at.%. The excitation with low-energy UV radiation only produces photoemission in the red side of the spectrum; when the energy is increased by an electric field (electroluminescence) or a beam of high-energy electrons (cathodeluminescence), emission in the whole range is presented. As the excitation energy increases, the emission shifts towards the blue side of the spectrum. Then, the emission wavelength can be selected as a function of applied energy, but presenting a minimum around 550 nm.

Acknowledgments

The authors appreciate the economic support of CONACYT. A. González-Fernández especially acknowledges Grant no. 213571. The authors also recognize the help of Ing. Pablo Alarcon.

References

[1] D. J. DiMaria, D. W. Dong, C. Falcony et al., "Charge transport and trapping phenomena in off-stoichiometric silicon dioxide films," *Journal of Applied Physics*, vol. 54, no. 10, pp. 5801–5827, 1983.

[2] D. Dong, E. A. Irene, and D. R. Young, "Preparation and some properties of chemically vapor-deposited Si-rich SiO and SigN, films," *Journal of the Electrochemical Society*, vol. 125, no. 5, pp. 819–823, 1978.

[3] X. X. Wang, J. G. Zhang, L. Ding et al., "Origin and evolution of photoluminescence from Si nanocrystals embedded in a SiO_2 matrix," *Physical Review B*, vol. 72, no. 19, Article ID 195313, 6 pages, 2005.

[4] D. J. DiMaria, J. R. Kirtley, E. J. Pakulis et al., "Electroluminescence studies in silicon dioxide films containing tiny silicon islands," *Journal of Applied Physics*, vol. 56, no. 2, pp. 401–416, 1984.

[5] A. Morales, J. Barreto, C. Domínguez, M. Riera, M. Aceves, and J. Carrillo, "Comparative study between silicon-rich oxide films obtained by LPCVD and PECVD," *Physica E*, vol. 38, no. 1-2, pp. 54–58, 2007.

[6] C. P. Poole Jr. and F. J. Owens, *Introduction to Nanotechnology*, Wiley-Interscience, New York, NY, USA, 2003.

[7] H. R. Philipp, "Optical and bonding model for non-crystalline SiO_x and SiO_xN_y materials," *Journal of Non-Crystalline Solids*, vol. 8–10, no. C, pp. 627–632, 1972.

[8] R. Alfonsetti, L. Lozzi, M. Passacantando, P. Picozzi, and S. Santucci, "XPS studies on SiOx thin films," *Applied Surface Science*, vol. 70-71, no. 1, pp. 222–225, 1993.

[9] D. Q. Yang, J. N. Gillet, M. Meunier, and E. Sacher, "Room temperature oxidation kinetics of Si nanoparticles in air, determined by x-ray photoelectron spectroscopy," *Journal of Applied Physics*, vol. 97, no. 2, Article ID 024303, 6 pages, 2005.

[10] E. Dehan, P. Temple-Boyer, R. Henda, J. J. Pedroviejo, and E. Scheid, "Optical and structural properties of SiO_x and SiN_x materials," *Thin Solid Films*, vol. 266, no. 1, pp. 14–19, 1995.

[11] Y. Liu, T. P. Chen, Y. Q. Fu et al., "A study on Si nanocrystal formation in Si-implanted SiO_2 films by x-ray photoelectron spectroscopy," *Journal of Physics D*, vol. 36, no. 19, pp. L97–L100, 2003.

[12] R. López-Estopier, M. Aceves-Mijares, and C. Falcony, "Cathodo- and photo- luminescence of silicon rich oxide films obtained by LPCVD," in *Cathodoluminescence*, N. Yamamoto, Ed., p. 324, InTech, 2012.

[13] J. A. Luna-López, M. Aceves-Mijares, O. Malik et al., "Compositional and structural characterization of silicon nanoparticles embedded in silicon rich oxide," *Revista Mexicana de Fisica*, vol. 53, no. 7, pp. 293–298, 2007.

[14] Z. Yu, M. Aceves-Mijares, and M. A. I. Cabrera, "Single electron charging and transport in silicon rich oxide," *Nanotechnology*, vol. 17, no. 15, article 059, pp. 3962–3967, 2006.

[15] D. Comedi, O. H. Y. Zalloum, E. A. Irving et al., "X-ray-diffraction study of crystalline Si nanocluster formation in annealed silicon-rich silicon oxides," *Journal of Applied Physics*, vol. 99, no. 2, Article ID 023518, 8 pages, 2006.

[16] X. Zhu, J. Zhu, A. Li, Z. Liu, and N. Ming, "Challenges in atomic-scale characterization of high-k dielectrics and metal gate electrodes for advanced CMOS gate stacks," *Journal of Materials Science and Technology*, vol. 25, no. 3, pp. 289–313, 2009.

[17] Z. Yu, M. Aceves, J. Carrillo, and R. López-Estopier, "Charge trapping and carrier transport mechanism in silicon-rich

silicon oxynitride," *Thin Solid Films*, vol. 515, no. 4, pp. 2366–2372, 2006.

[18] A. Morales-Sánchez, J. Barreto, C. Domínguez-Horna, M. Aceves-Mijares, and J. A. Luna-López, "Optical characterization of silicon rich oxide films," *Sensors and Actuators, A*, vol. 142, no. 1, pp. 12–18, 2008.

[19] F. Iacona, C. Bongiorno, C. Spinella, S. Boninelli, and F. Priolo, "Formation and evolution of luminescent Si nanoclusters produced by thermal annealing of SiOx films," *Journal of Applied Physics*, vol. 95, no. 7, pp. 3723–3732, 2004.

[20] F. Ay and A. Aydinli, "Comparative investigation of hydrogen bonding in silicon based PECVD grown dielectrics for optical waveguides," *Optical Materials*, vol. 26, no. 1, pp. 33–46, 2004.

[21] P. G. Pai, S. S. Chao, Y. Takagi, and G. Lucovsky, "Infrared spectroscopic study of SiOx films produced by plasma enhanced chemical vapor deposition," *Journal of Vacuum Science & Technology A*, vol. 4, no. 3, pp. 689–694, 1986.

[22] N. Daldosso, G. Das, S. Larcheri et al., "Silicon nanocrystal formation in annealed silicon-rich silicon oxide films prepared by plasma enhanced chemical vapor deposition," *Journal of Applied Physics*, vol. 101, no. 11, Article ID 113510, 7 pages, 2007.

[23] F. Iacona, G. Franzò, and C. Spinella, "Correlation between luminescence and structural properties of Si nanocrystals," *Journal of Applied Physics*, vol. 87, no. 3, pp. 1295–1303, 2000.

[24] E. Fazio, E. Barletta, F. Barreca, F. Neri, and S. Trusso, "Investigation of a nanocrystalline silicon phase embedded in SiO_x xthin films grown by pulsed laser deposition," *Journal of Vacuum Science and Technology B*, vol. 23, no. 2, pp. 519–524, 2005.

[25] B. Valeur and M. N. Berberan-Santos, "A brief history of fluorescence and phosphorescence before the emergence of quantum theory," *Journal of Chemical Education*, vol. 88, no. 6, pp. 731–738, 2011.

[26] N. Meriç, M. A. Atlihan, M. Koşal, Ü. R. Yüce, and A. Cinaroglu, "Infrared stimulated luminescence and thermoluminescence dating of archaeological samples from Turkey," *Geochronometria*, vol. 34, no. 1, pp. 25–31, 2009.

[27] T. M. Piters, M. Aceves-Mijares, D. Berman-Mendoza, L. R. Berriel-Valdos, and J. A. Luna-López, "Dose dependent shift of the TL glow peak in a silicon rich oxide (SRO) film," *Revista Mexicana De Física S*, vol. 57, no. 2, pp. 26–29, 2011.

[28] L. T. Canham, "Silicon quantum wire array fabrication by electrochemical and chemical dissolution of wafers," *Applied Physics Letters*, vol. 57, no. 10, pp. 1046–1048, 1990.

[29] M. Ray, S. M. Hossain, R. F. Klie, K. Banerjee, and S. Ghosh, "Free standing luminescent silicon quantum dots: evidence of quantum confinement and defect related transitions," *Nanotechnology*, vol. 21, no. 50, Article ID 505602, 2010.

[30] M. N. Islam and S. Kumar, "Influence of surface states on the photoluminescence from silicon nanostructures," *Journal of Applied Physics*, vol. 93, no. 3, pp. 1753–1759, 2003.

[31] G. Franzò, A. Irrera, E. C. Moreira et al., "Electroluminescence of silicon nanocrystals in MOS structures," *Applied Physics A*, vol. 74, no. 1, pp. 1–5, 2002.

[32] A. Irrera, D. Pacifici, M. Miritello et al., "Excitation and deexcitation properties of silicon quantum dots under electrical pumping," *Applied Physics Letters*, vol. 81, no. 10, pp. 1866–1868, 2002.

[33] M. Cervera, M. J. Hernández, P. Rodríguez et al., "Blue-cathodoluminescent layers synthesis by high-dose N^+, C^+ and B^+ SiO_2 implantation," *Journal of Luminescence*, vol. 117, no. 1, pp. 95–100, 2006.

[34] A. Kalnitsky, J. P. Ellul, E. H. Poindexter, P. J. Caplan, R. A. Lux, and A. R. Boothroyd, "Rechargeable E' centers in silicon-implanted SiO_2 films," *Journal of Applied Physics*, vol. 67, no. 12, pp. 7359–7367, 1990.

[35] M. Aceves, C. Falcony, A. Reynoso-Hernandez, W. Calleja, and A. Torres, "The conduction properties of the silicon/off-stoichiometry-SiO_2 diode," *Solid-State Electronics*, vol. 39, no. 5, pp. 637–644, 1996.

[36] Z. Yu, M. Aceves, F. Wang, J. Carrillo, R. Kiebach, and K. Monfil, "Room temperature quantum tunneling and Coulomb blockade in silicon-rich oxide," *Physica E*, vol. 41, no. 2, pp. 264–268, 2008.

[37] J. Heitmann, F. Müller, M. Zacharias, and U. Gösele, "Silicon nanocrystals: size matters," *Advanced Materials*, vol. 17, no. 7, pp. 795–803, 2005.

[38] J. Zhong Zhang, *Optical Properties and Spectroscopy of Nanomaterials*, chapter 5, Scientific, Norwood, NJ, USA, 2009.

[39] M. H. Nayfeh, S. Rao, O. M. Nayfeh, A. Smith, and J. Therrien, "UV photodetectors with thin-film Si nanoparticle active medium," *IEEE Transactions on Nanotechnology*, vol. 4, no. 6, pp. 660–668, 2005.

[40] J. Valenta, P. Janda, K. Dohnalová, D. Nižňansky, F. Vácha, and J. Linnros, "Colloidal suspensions of silicon nanocrystals: from single nanocrystals to photonic structures," *Optical Materials*, vol. 27, no. 5, pp. 1046–1049, 2005.

[41] M. V. Wolkin, J. Jorne, P. M. Fauchet, G. Allan, and C. Delerue, "Electronic states and luminescence in porous silicon quantum dots: the role of oxygen," *Physical Review Letters*, vol. 82, no. 1, pp. 197–200, 1999.

[42] A. Morales-Sánchez, J. Barreto, C. Domínguez, M. Aceves, and J. A. Luna-López, "The mechanism of electrical annihilation of conductive paths and charge trapping in silicon-rich oxides," *Nanotechnology*, vol. 20, no. 4, Article ID 045201, 2009.

[43] A. A. G. Fernández, M. A. Mijares, A. M. Sánchez, and K. M. Leyva, "Intense whole area electroluminescence from low pressure chemical vapor deposition-silicon-rich oxide based light emitting capacitors," *Journal of Applied Physics*, vol. 108, no. 4, Article ID 043105, 2010.

[44] H. S. Nalwa and L. S. Rohwer, Eds., *Handbook of Luminescence, Display Materials, and Devices, Volume 1 Organic Light-Emitting Diodes*, American Scientific, Valencia, Calif, USA, 2003.

[45] R. López-Estopier, M. Aceves-Mijares, Z. Yu, and C. Falcony, "Determination of the energy states of the donor acceptor decay emission in silicon rich oxide prepared by low-pressure chemical vapor deposition," *Journal of Vacuum Science and Technology B*, vol. 29, no. 2, Article ID 021017, 5 pages, 2011.

[46] B. G. Yacobi and D. B. Holt, *Cathodoluminescence Microscopy of Inorganic Solids*, Plenum Press, New York, NY, USA, 1990.